

The Corrosion Process of an API 5L X80 Welded Joint in a System with Different pH and H₂S Concentration

M. B. L. Carvalho^{a*} , I. S. Bott^a , A. B. Forero^b, J. A. C. Ponciano^c 

^aPontifícia Universidade Católica do Rio de Janeiro, Departamento de Engenharia Química e de Materiais, Rua Marquês de São Vicente, 225, Gávea, 22453-900, Rio de Janeiro, RJ, Brasil.

^bCompañía Massy Energy Colombia, Cra. 45^a n° 93-64, Bogotá, Colombia.

^cUniversidade Federal do Rio de Janeiro, Centro de Tecnologia, Departamento de Engenharia Metalúrgica e de Materiais, Laboratório de Corrosão (LabCorr), Avenida Horácio Macedo, 2030, Bloco F, Cidade Universitária, 21941-598, Rio de Janeiro, RJ, Brazil.

Received: September 03, 2021; Revised: December 16, 2021; Accepted: December 22, 2021

The corrosion evaluation of steels in the oil and gas industry environments is a crucial issue because corrosion can cause economic and human losses. It is well known that H₂S can be originated from different processes in the oil and gas industry, accelerating the corrosion process. The objective of this work was to evaluate the H₂S corrosion resistance of an API 5L X80 steel and its welded joint obtained by submerged arc welding process (SAW). All tests were performed in an aerated 5% wt NaCl and thiosulphate aqueous solution. The H₂S concentration, pH, weight loss, electrochemical tests, and microstructure were considered. The results obtained showed an increase of the corrosion rate values, with decreasing pH and increasing concentration of H₂S generated by the thiosulphate. For the lowest H₂S concentrations, the corrosion process was inhibited, due to the formation of a partially protective film on the samples' surfaces. The heat affected zone (HAZ) showed severe localized corrosion attack which was attributed to the microstructural characteristics of this region.

Keywords: Corrosion, H₂S, API 5L X80, Welded joint, Electrochemical tests, Weight loss tests.

1. Introduction

The deterioration of a buried metal that has been submerged or exposed to industrial environments represents a real problem for the economy and the environment. It is well known that H₂S originating from different processes in the oil and gas industry can accelerate anodic and cathodic reactions of the corrosion process^{1,2}. The H₂S corrosion resistance properties of steels depend not only upon the steel cleanliness, but also on its microstructure³⁻¹¹. The welding procedures adopted during the production of the tubes and for construction of the pipelines can modify its microstructure and, consequently, the mechanical and corrosion properties of the base metal in the heat affected zone (HAZ). These changes can increase the corrosion attack in these specific zones¹¹⁻¹⁷. Corrosion rates of low alloy steels in H₂S containing environment tend to increase with increasing H₂S concentration and decreasing pH of the aqueous solution¹⁸.

In the present work, weight loss tests and electrochemical tests (linear polarization resistance (LPR), Tafel curves (TC) and electrochemical impedance spectroscopy (EIS)) were used to calculate the corrosion rate, in order to investigate the effect of H₂S concentration and pH of system pH on the corrosion process of an API 5L X80 steel and its SAW welded joint. The results obtained showed that the corrosion rate accomplished for both base metal (BM)

and the welded joint (WJ) increased with the decreasing pH, regardless of the H₂S concentration generated by the thiosulphate.

In this work, the corrosion process was inhibited for the lowest H₂S concentration, causing a significant decrease in the corrosion rate. This effect could be a result of a partially protective film formed on the samples' surface for the solution with low H₂S concentration. However, a more severe attack in the HAZ was present, indicating an influence of the microstructure on the corrosion attack mechanism.

2. Experimental Procedure

2.1. Materials

The material of this study was an API 5LX80 steel. Samples of base metal and welded joint (weld metal and heat affected zone (HAZ)) were taken from a tube welded longitudinally by submerged arc welding (SAW) process, as shown in Figure 1.

The average values of the chemical composition (Table 1), sampled from two different points of the BM and the WJ, were obtained using the optical emission spectroscopy technique according to ASTM E 415-2008.

Microstructural analyses, using Optical Microscopy Zeiss Axioskop (OM), were performed, and the samples

*e-mail: nickcarvalho9@gmail.com

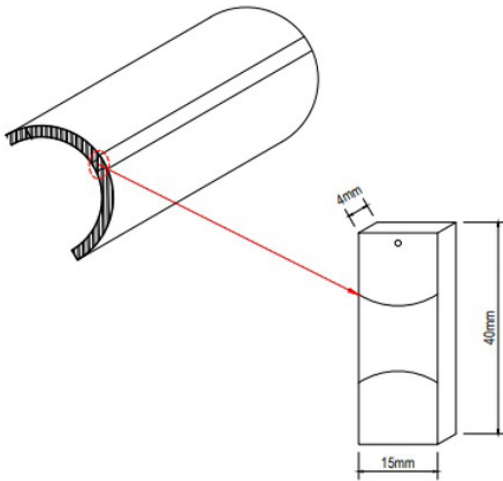


Figure 1. Specimen dimensions in mm.

Table 1. Chemical Compositions of the base metal and weld metal in wt%.

Element	Base Metal (%) wt content	Weld Metal (%) wt content	API 5L Max (%) wt content
C	0,058	0,056	0,22
Si	0,203	0,273	-
Mn	1,71	1,59	1,85
P	0,023	0,027	0,025
S	0,0031	0,0062	0,015
Cr	0,131	0,100	-
Ni	0,020	0,023	-
Mo	0,192	0,178	-
Al	0,044	0,021	-
Cu	0,011	0,050	-
Co	<0,0015	<0,0015	-
Ti	0,015	0,014	c, d
Nb	0,064	0,037	c, d
V	0,023	0,017	c, d
B	0,0007	0,0027	-
Ca	0,0032	0,0016	-
Fe	Balance	Balance	-

c Niobium, Vanadium, Titanium, or combinations thereof may be used at the discretion of the manufacturer; d Sum of the Niobium, Vanadium, and Titanium contents not exceed 0, 15% (API 5L, 2007).

were prepared using the conventional method of grinding and etching with a 2% Nital solution for 5 to 10 seconds. Electrolytic double etching technique was also used to adequately reveal the presence of martensite and austenite microconstituent (MA) for Scanning Electron Microscopy JEOL (JSM-6510L) (SEM) analysis, as shown in Figure 2.

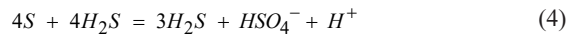
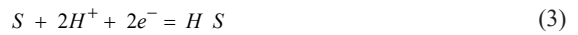
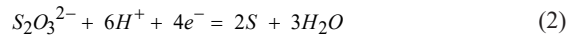
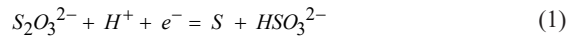
2.2. Weight loss tests

The effect of pH, H_2S concentration and microstructural characteristics on the corrosion rate and corrosion products morphology were studied using the weight loss technique in a 5%wt NaCl brine and different corrosive environments based on a sodium thiosulphate solution, as listed in Table 2.

H_2S was indirectly generated by the reaction of the Sodium thiosulfate solutions at the interface electrolyte/metal, at atmospheric pressure and room temperature according to the reactions⁷:

Table 2. Chemical composition of the solutions used in electrochemical techniques.

Solution	Sodium Thiosulphate ($Na_2S_2O_3$)	Sodium Chloride (NaCl)	pH
Brine	0		
Solution 1	10^{-3} mol/L		5.0
Solution 2	10^{-2} mol/L		
Brine	0	5%wt	
Solution 1	10^{-3} mol/L		3.0
Solution 2	10^{-2} mol/L		



The specimens of 40x15x4 mm dimension were washed, grounded using a 220 to 600 grit sandpaper and weighed prior to the test. Three samples of each region (base metal and welded joint) were immersed in the solution for 30 days and tested for the same conditions, as described in Table 2.

After the end of the test and removal of the sample from the solution, the corrosion products were detached from the specimen surface and followed by cleaning, drying and re-weighing according to ASTM G1-03(2011) standard¹⁹. The corrosion rate was an average of the results obtained from three different samples, using the Equation 5, where K = a constant = 3.45×10^6 , W = mass loss in g, A = Area in cm^2 , T = time in hours and D = density in g/cm^3 (7.85).

$$Corrosion\ Rate\ (mpy) = \left(\frac{K * W}{A * T * D} \right) \quad (5)$$

Visual, optical (OM) and scanning electron microscopy (SEM) analyses of the sample surfaces were performed to determine the type and morphology of the corrosion process.

2.3. Electrochemical techniques

Linear Polarization Resistance (LPR) tests, Tafel polarization curves (TP) and Electrochemical Impedance Spectroscopy (EIS) were applied using different corrosive environments (Table 2), in a typical electrochemical cell of three electrodes, using platinum as the counter electrode and a standard silver/silver chloride electrode (Ag/AgCl) as reference.

In the LPR test, the triplicate specimens were placed in the electrochemical cell to come in contact with test solution. The specimens were kept immersed in the solution for 3 hours, maintaining the system in open circuit to obtain the stabilization of the corrosion potential (E_{corr}). LPR measurements were carried out by polarizing the specimen from +20 to -20 mV in respect to E_{corr} , with scanning rate of 0.6 V / hour, as specified in ASTM G-59-2003²⁰.

$$R_p = \left[\frac{d(\Delta E)}{di} \right]_{\Delta E=0} \quad (6)$$

Where ΔE = the difference $E - E_{\text{corr}}$, and R_p = polarization resistance in ($\Omega \cdot \text{cm}^2$).

After recording the LPR tests, in order to reach stabilisation, the system was kept at open circuit potential for approximately two hours. Electrochemical impedance spectroscopy (EIS) was carried out at E_{corr} , using a 10 mV signal amplitude and a frequency range of 100 kHz to 0.01 Hz.

Tafel polarization curve test was applied using a scanning potential of 250 mV above and below the open circuit potential (E_{corr}), approximately 24 hours after immersion. The logarithm of current density obtained was plotted as a function of scanning potential (E vs. $\log I$). From these curves anodic and cathodic Tafel slopes (ba and bc) were obtained.

The corrosion current density was calculated, using the Stern-Geary equation:

$$I_{\text{corr}} = \frac{B}{R_p} \quad (7)$$

$$B = \frac{(abc)}{2.303(ba + bc)} \quad (8)$$

Where I_{corr} = corrosion current density in $\mu\text{A}/\text{cm}^2$, ba and bc are given in mV/decade, R_p = polarization resistance ($k\Omega \cdot \text{cm}^2$).

The corrosion rate was obtained by the following relationship:

$$R_{\text{corr}} = \frac{(0.13I_{\text{corr}}PE)}{\rho} \quad (9)$$

Where R_{corr} = corrosion rate in mpy, PE = equivalent weight of metal in g, ρ = density of metal in g/cm^3 (7.85 for low alloy steel)

3. Results and Discussion

The Figure 2 shows the base metal exhibited a ferritic matrix with MA microconstituent. The weld metal microstructure was mainly acicular ferrite and grain boundary ferrite and the heat affected zone (HAZ), regardless of the region, usually exhibited ferrite bainitic microstructure with decomposed MA microconstituent. Some regions of the fine grain HAZ display polygonal and almost polygonal ferrite.

The average corrosion rates (Figure 3) were obtained from weight loss tests of both regions (base metal and welded joint) in different H₂S containing solutions. An increase of the corrosion rates with the decreasing pH of the solution is shown, this effect being more significant for solution 2. For most steels in H₂S-containing environments, the corrosion rates tend to increase with decreasing pH of the aqueous solution²¹. The stable form of H₂S depends upon the solution acidity (pH), therefore, H₂S is stable as a dissolved species in aqueous solutions only at low pH levels ($\text{pH} \leq 6$); whereas at higher pH levels (between 7 and 11) the predominant form is HS⁻, and for alkaline pH values the stable form is S²⁻.

ASTM D 2688-11²² specifies that uniform corrosion rates smaller than 0.13 mm/y are considered low and are a general indication of adequate service life for metals tested and exposed to pipeline systems. As can be seen in Figure 3, the values of corrosion rate obtained for both base metal and the welded joint, in brine and in solution 2, with $\text{pH} = 5.0$ and 3.0, respectively, indicate a severe degradation.

All the values obtained for the specimens tested in Solution 1 are below the limit specified in the standard ASTM D 2688-11. These results are not expected since this system contains H₂S generated by the reaction of sodium thiosulphate with the metal surface. However, corrosion rates higher than those obtained in brine would be expected.

The influence of hydrogen sulphide on the steel corrosion, in the vast majority of the cases, showed that the increase in the H₂S concentration increases the corrosion rate^{1,21,23-25}, due to the fact the both processes anodic dissolution and hydrogen evolution are accelerated. However, under certain special operating conditions where H₂S concentrations are low (<0.04 mmol/l, <15 ppm or <0.05 psi), pH values

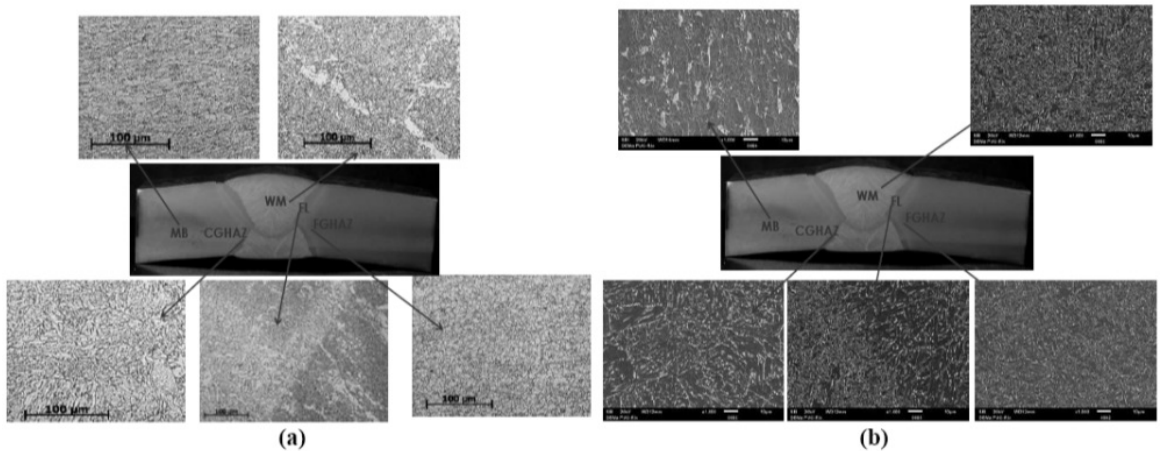


Figure 2. Microstructural Characterization of welded joint. (a) OM (b) SEM.

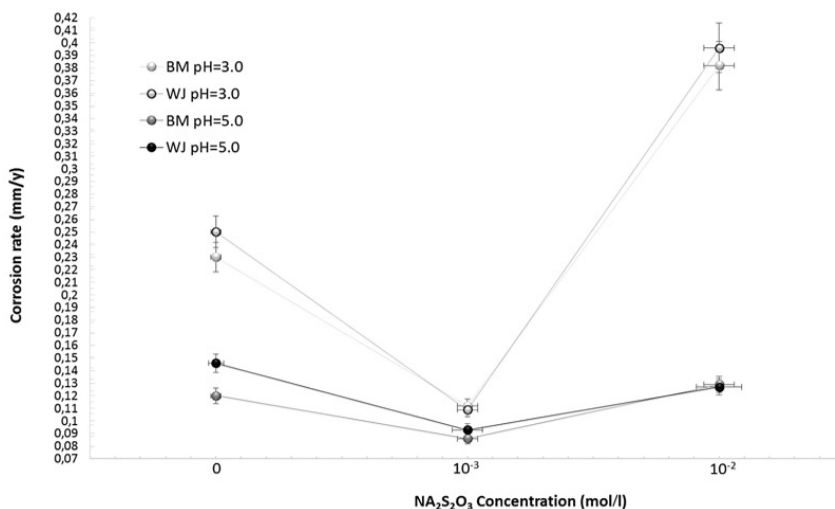


Figure 3. Average corrosion rates obtained by loss weight tests from different solutions.

between 3-5, and immersion times are exceeding two hours, the corrosion process can be inhibited, causing a significant decrease in the corrosion rate¹⁻²³, as shown by the results obtained for the solution 1 in this study.

In general, iron corrosion in H_2S -containing solutions leads to the formation of a Fe_xS_y film, where the type of sulphide depends on the H_2S concentration in the solution. Considering the H_2S concentration of the solutions in this work, the corrosion rate was lower for the solution 1 and higher for solution 2. This effect is thought to be caused by the formation of a partially protective film on the samples in solutions with low H_2S concentration²⁵. Corrosion product layers were formed for all conditions tested, however, apparently, for solution 1 (pH=3.0), the layer formed was compact and the metal surface was isolated, thus avoiding the corrosion attack. Figure 4 shows the surface appearance of the specimens that were tested for weight loss before the removal of corrosion products.

Gravimetric analysis associated with quantitative information allows the identification of the type of corrosion that occurs within the system. After the end of each test, the specimens were removed from the cell, manually washed, dried and weighed in accordance with ASTM G1-03(2011) standard. Visual analysis of the samples surface was performed before and after washing, and after the removal of corrosion products, in order to identify the form of corrosion in each medium. The most representative visual aspect of the various systems tested is shown in Figure 5.

For brine tests with pH=5.0, the corrosion was uniform along the sample surface. For pH=3.0, the corrosion was both uniform and localised (pitting), showing a higher pit density in the HAZ at coarse and fine grain regions, as shown in Figures 4.

In general, the samples that submerged in solutions 1 and 2 showed uniform and localised corrosion. The most affected region for pitting corrosion was the HAZ; the preferential attack was more intense for solution 2 where sodium thiosulphate concentration is higher, and pH=3.0, indicating that this solution provides more severe environment.

Detailed SEM analysis showed the selective attack, localised pitting and alveolar types of corrosion at the HAZ and base metal (Figures 6-8). The coarse grain zone of the HAZ is the most affected, possibly due to the microstructural transformations present in this region.

The greatest degradation occurred in the ferrite-bainitic microstructure, as corresponding to the elongated ferrite, and within the partially decomposed microconstituent AM, as related to the ferrite and carbide aggregates. The dark areas probably correspond to clusters of ferrite, while the lighter areas correspond to an aggregate of precipitate and carbides. While the dark areas are more attacked and the lighter areas which have an embossed appearance do not appear to be attacked.

In a corrosive medium containing thiosulphate, the interaction of the environment with the metal surface⁷ generates H_2S and, as soon as the cathodic and anodic reactions occur, a layer of corrosion products will be formed. Initially, this layer must be constituted of iron sulphate and oxides and can have protective qualities. However, the observed tendency was a porous and brittle layer. Additionally, this layer can be dissolved by the acid dilution. Therefore, the areas where the layer is broken or weakened can become available to react with the medium and produce H_2S in the areas adjacent to the metal surface. This sequence of events leads to a localised attack in these areas, as can be observed in Figures 6-8.

In this work, an increase in the corrosion rate was observed for solution 2 (pH=3.0), which indicates that the formed film was not protective under these conditions. For solution 1, a decrease in the corrosion rate was observed for the two studied pH values, which indicates the formation of a film that inhibits the corrosion process of the metal. Thus, the structure and composition of the films were determined using electron dispersive spectroscopy (EDS) and X-ray diffraction analysis (XRD), shown in Figures 9-12.

The formed films have a discontinuous and porous morphology and were formed mainly of oxides, sulfides and chlorides, as you identify in the EDS spectra. For the specimen tested in solution 2 with pH = 3.0, visual inspection

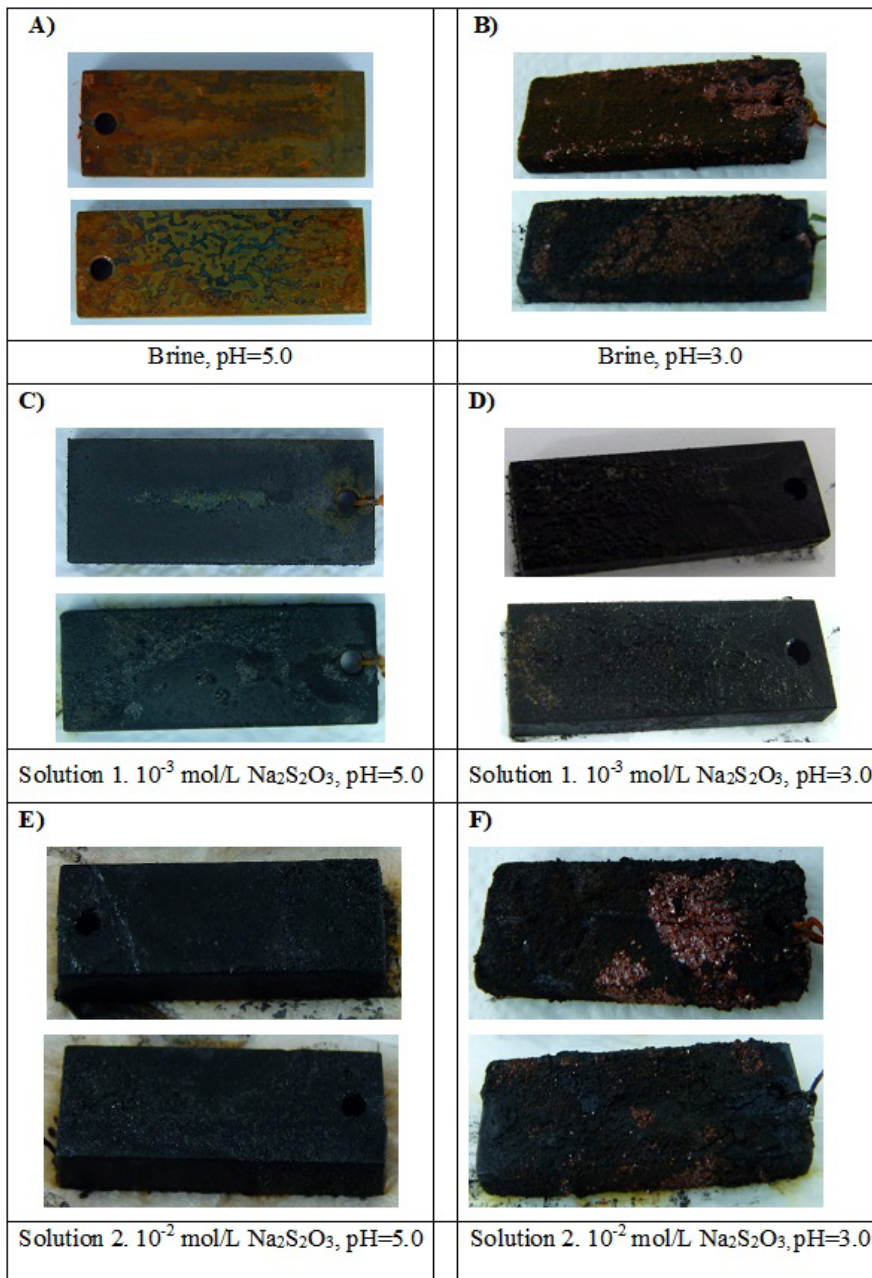


Figure 4. Surface aspect of the weight loss test specimens before removal of corrosion products.

(Figure 4f) suggests the presence of two layers: the first layer grows adjacent to metal surface, an irregular and black layer, showing some degree of porosity. The second layer consists of crystal clusters with a columnar geometry of possibly a more stable iron sulfide, as suggested by EDS spectrum.

Figure 9 shows the EDS spectra from different areas of the layer formed on the surface of the welded joint. The first layer shows the presence of Fe, Cl, Ni, Na, Mn and O, whereas the second layer (columnar crystal) is mainly composed of S, Fe, and Na. The spectra obtained from the layers that were apparently formed first indicate the presence of oxygen. It can be said that an oxide layer was initially formed and became a type of meta-stable sulphide (mackinawite), crystals with

columnar geometry, which appears to be a type of sulphide enriched in sulphur. This assessment is supported by the XRD spectrum shown in Figure 10.

The corrosion film that formed for the WJ in solution 1 with pH=3.0 (Figure 10) has different morphologies from that formed in solution 2. This film exhibits an inner layer with a continuous and compact morphology adjacent to the metallic substrate surface and an outer layer with a discontinuous, porous and granular morphology above the inner layer. The EDS spectra (Figure 11) and XRD spectrum (Figure 12) show that the inner layer may be an iron oxide (magnetite or maghemite), and the outer layer may be an iron sulphide (mackinawite).

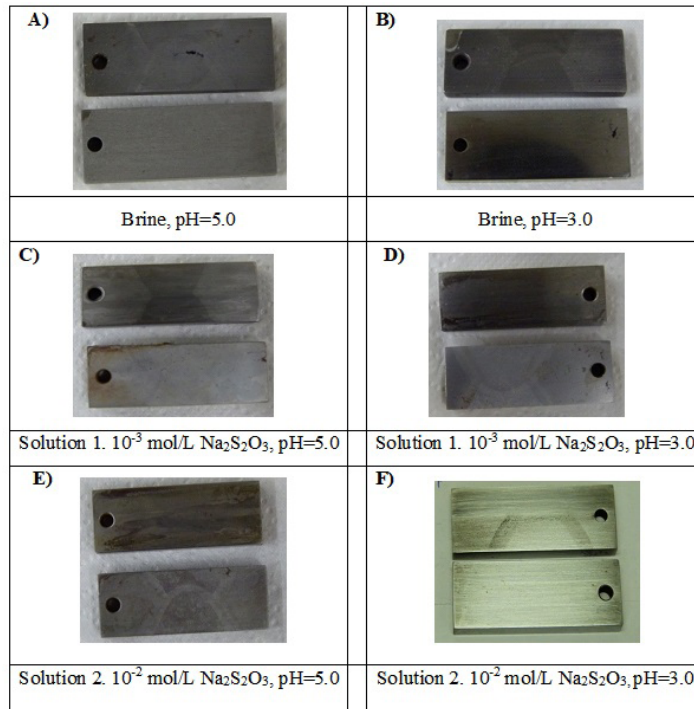


Figure 5. Surface aspect of the weight loss test specimens after removal of corrosion products.

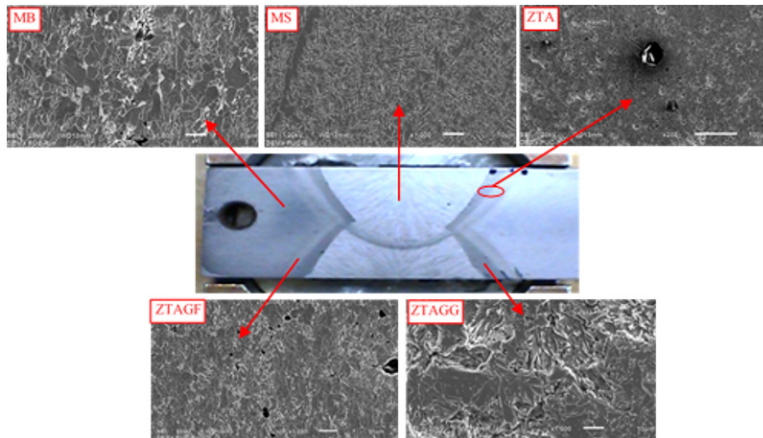


Figure 6. SEM surface characterization of a sample tested in brine (pH=3.0) after immersion for 30 days.

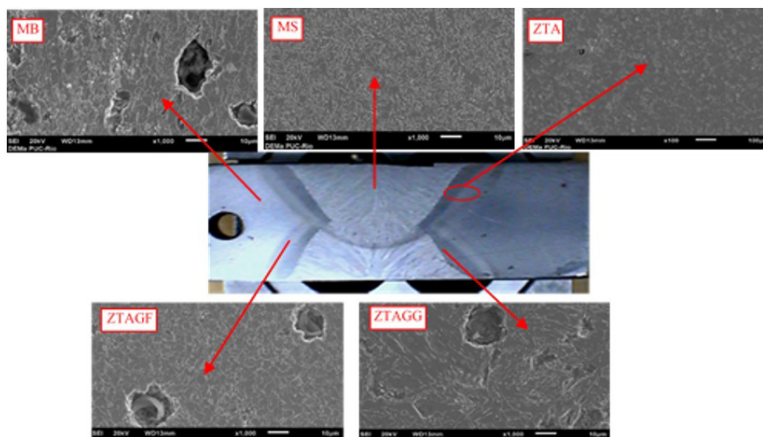


Figure 7. SEM surface characterization of the sample after 30 days immersion at solution 1 (10^{-3} mol/L $\text{Na}_2\text{S}_2\text{O}_3$) (pH=3).

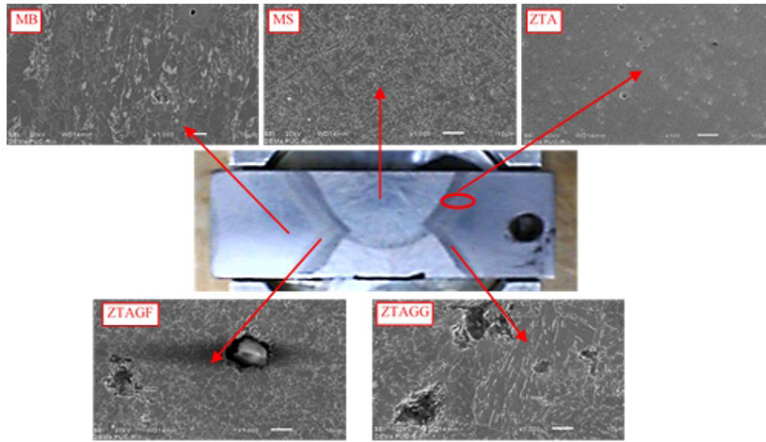


Figure 8. SEM surface characterization of the sample after 30 days immersion in solution 2 (10^{-2} mol/L Na₂S₂O₃) (pH=3.0).

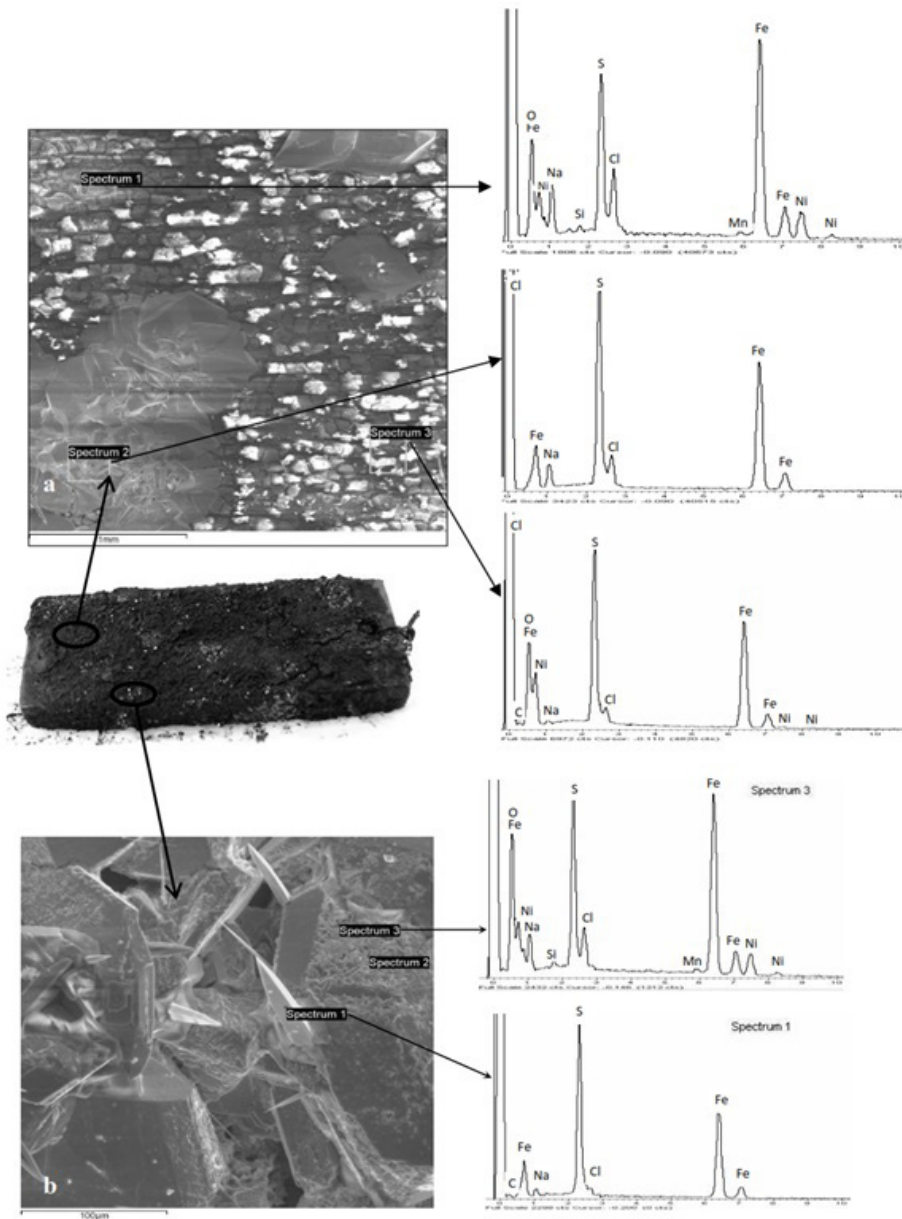


Figure 9. SEM and EDS characterization of the corrosion product film on the surface of the welded joint that was tested in solution 2 with pH=3.0.

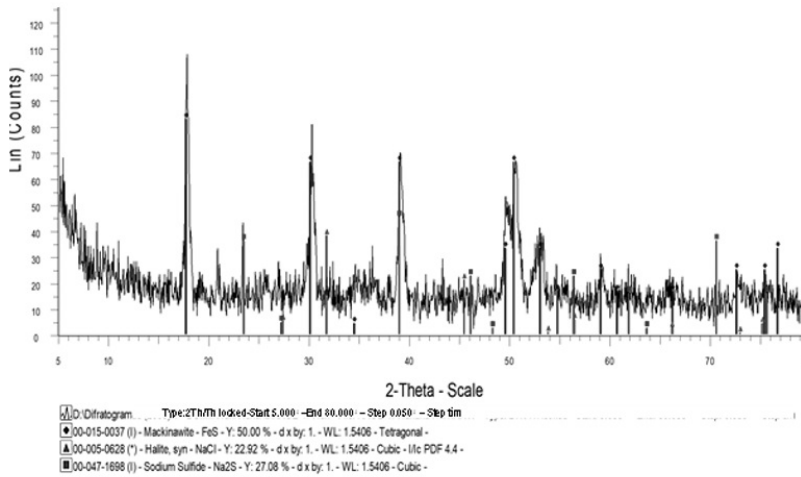


Figure 10. XRD spectrum of the corrosion product film of the welded joint that was tested in in solution 2 with pH=3.0

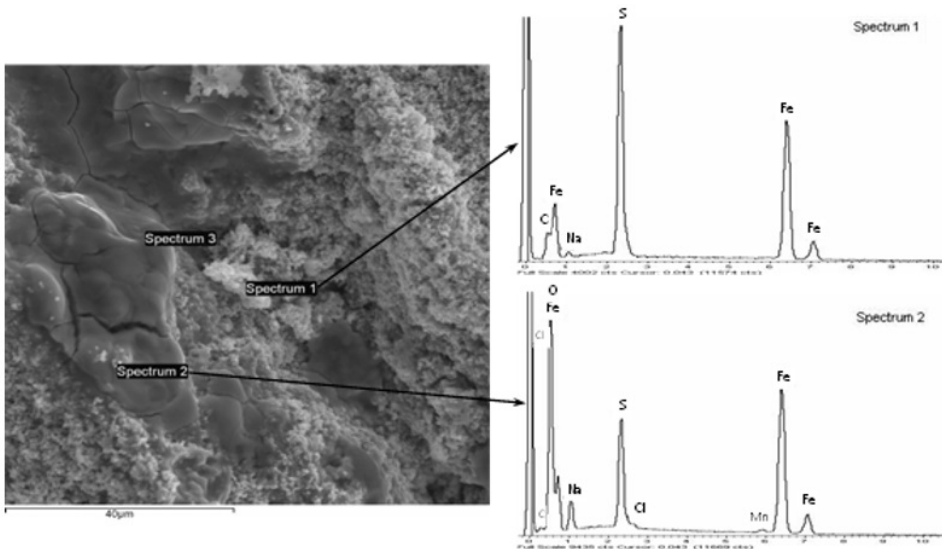


Figure 11. SEM and EDS characterization of the corrosion product film of the welded joint that was tested in solution 1 with pH=3.0.

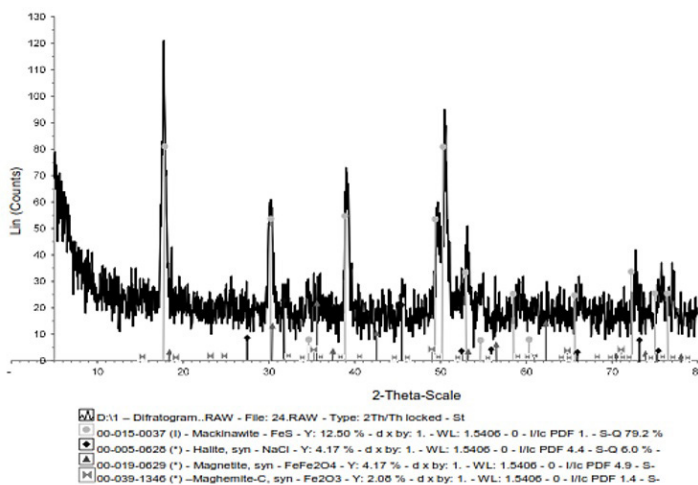


Figure 12. XRD spectrum of the corrosion product film of the welded joint that was tested in solution 1 with pH=3.0.

The corrosion films that formed for solution 1 exhibit a more regular and compact morphology, which contributes to the formation of protective layers and thus decreases the corrosion rate.

Figure 13 shows the characteristic curves of LPR measured at different environments with additions of sodium thiosulfate (Na₂S₂O₃) for both base metal and welded joint. Comparing the linear polarization resistance curves for the different environments, the curve slope increases with increasing sodium thiosulphate concentration. As RPL parameter is indirectly proportional to the corrosion rate, there is an indication of a higher corrosion rate for environments with higher H₂S concentration.

At the anodic polarization of Tafel curves (Figure 14), which represents the anodic reaction of the corrosion process, active dissolution was observed. The cathodic curves behaviour in the brine is characterised by a smoothed limiting diffusion current density, indicating a process of reducing a compound dominant, this process being dependent on the potential. For our case, it indicates starting the process reduction of H⁺ ion.

For the solutions containing sodium thiosulphate, the cathodic curves show the current limit more marked and this behaviour can be attributed to the process of formation of H₂S in the system and the start of the H⁺ ion reduction.

Similar results were obtained by Lucio-Garcia et al.²⁴, who studied the H₂S corrosion resistance of a microalloyed steel with three different heat treatments and microstructures. The addition of Na₂S₂O₃ and generation of H₂S in the system is reflected in all the curves obtained for solutions 1 and 2, in each case the whole curve being moved towards higher current density values compared to those obtained for the brine solution (Figure 14).

The most representative Nyquist diagrams for the different environments studied with pH=5.0 are shown in Figure 15. At higher frequencies, the capacitive semi-circles formed, for both base metal and welded joint in the thiosulphate solutions were similar to the capacitive arc formed for the brine, although smaller, for most tests. The semicircles obtained for the solutions containing thiosulphate showed a decrease in diameter, indicating that there is a decrease in the polarisation resistance (R_p) and, therefore, an increase in the corrosion rate for these environments, as indicated previously by the LPR tests.

EIS is also used to investigate corrosion mechanisms²⁶⁻²⁹. In this work, the Nyquist plots obtained showed one capacitive loop at high frequency and one inductive loop at lower frequency values. This corresponds to a process of charge transfer for high frequencies and followed by a diffusion

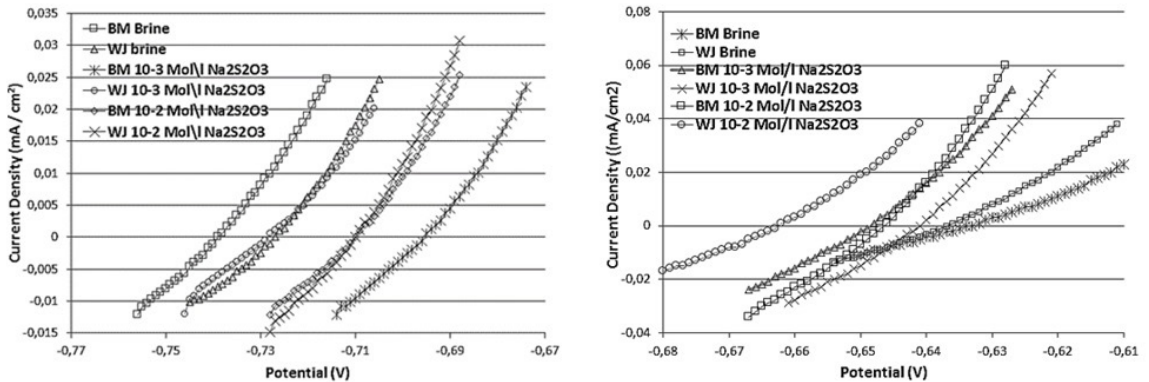


Figure 13. Characteristic LPR Curves of BM and WJ in different environments with: a) pH=5.0 and b) pH=3.0, respectively.

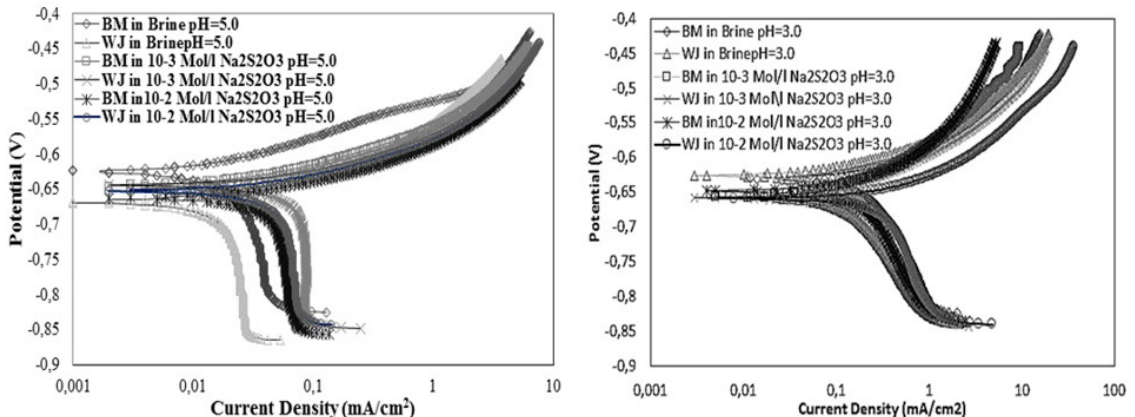


Figure 14. Characteristic Tafel Curve for the base metal and welded joint in different environments with: a) pH=5.0 and b) pH=3.0, respectively.

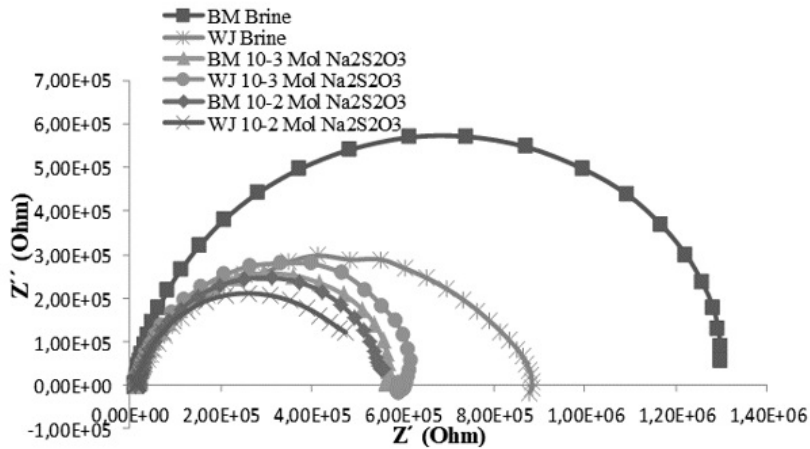


Figure 15. Characteristic Nyquist diagrams in different environments.

controlled process for lower frequencies (adsorption and dissolution of species or a nucleation stage of the scale formation process)²⁹.

At lower frequencies, the Nyquist diagrams for the welded joint showed the formation of an inductive arc, this may be related to the dissolution of the iron sulfide film. However, Ma et al.¹ attributed the formation of the inductive arc to the non-formation of a protective film, which disappears with the increase in immersion time, that is, this arc disappears as the sulfide film is generated on the metal surface.

Similar spectra were obtained by Choi et al.²⁶, who investigated the mechanism of iron sulphide scale formation in $\text{CO}_2/\text{H}_2\text{S}$ environments and evaluated the effect of added H_2S on CO_2 corrosion of carbon steel in acidic solutions. When 100ppm H_2S was added into the CO_2 environment, an increase of the R_p obtained from LPR and the diameter of semicircles from EIS was observed, causing an immediate decrease in the corrosion rate. They attributed this phenomenon to the formation of a protective iron sulphide film on the steel surface. On the other hand, when H_2S was completely removed from the CO_2 environment, the R_p obtained from LPR and the diameter of semicircles from EIS decreased, and the corrosion rate returned to its previous levels. They suggested that this phenomenon was due to the dissolution of the iron sulphide.

The H_2S corrosion process tends to form iron sulphide (Fe_xS_y) films and, although this film can facilitate hydrogen

permeation, it can also act as a physical barrier between the metal and the medium, reducing corrosion rate²⁶. These films can vary widely in composition and stoichiometry, therefore the protective effect is dependent on the conditions of the environment in which they are formed (pH, concentration of sulphates, presence of chlorides, time of formation, liquid or gas phase and microstructure of the substrate)^{2,4,6,7,11,17,24,26}. In the present case, for both techniques used RPL and EIS, an increase of the corrosion rate was observed, indicating that the film formed was not protective.

The average values for corrosion rates calculated by the two techniques used (EIS and LPR) are in good agreement, and are shown in the Table 3. The corrosion rate values increase with increasing concentration of H_2S generated by the thiosulphate. The welded joint showed higher corrosion rate in comparison with those presented by the base metal, for all conditions studied.

Comparing the results obtained for weight loss and electrochemical tests, it can be seen that the samples' immersion time is determinant in the process of layer formation and in its protective characteristics. The electrochemical tests with 24 hours' duration did not produce protective layers for all different conditions tested. On the other hand, for the weight loss tests for the samples immersed for 30 days, there was formation of protective layers for solution 1 (10^{-2} mol/L $\text{Na}_2\text{S}_2\text{O}_3$) for both pH tested.

Table 3. Average corrosion rates values obtained by loss weight tests, LPR and EIS techniques.

Environment	Material	RP DC ($\Omega\cdot\text{cm}^2$)	RP AC ($\Omega\cdot\text{cm}^2$)	C. Tafel B (V/dec)	ba (V/dec)	bc (V/dec)	Icorr DC ($\mu\text{A}/\text{cm}^2$)	Icorr AC ($\mu\text{A}/\text{cm}^2$)	Vcorr DC (mm/y)	Vcorr AC (mm/y)
Brine 5%wt NaCl	BM	888,96	933.57	0.022	0.06	0.381	25,32	25.32	0.297	0.282
	WJ	596.98	586.04	0.019	0.051	0.368	32.58	32.26	0.382	0.391
Solution 1 10^{-3} mol/L de $\text{Na}_2\text{S}_2\text{O}_3$	BM	492.89	432.84	0.018	0.05	0.269	36.93	42.31	0.434	0.502
	WJ	471.05	410.58	0.019	0.054	0.279	41.49	47.83	0.487	0.563
Solution 2 10^{-2} mol/L de $\text{Na}_2\text{S}_2\text{O}_3$	BM	392.26	343.99	0.017	0.046	0.249	42.99	49.01	0.505	0.581
	WJ	392.36	341.84	0.018	0.048	0.312	46.45	52.82	0.545	0.620

4. Conclusions

The results obtained by the two techniques used (loss weight and electrochemical test) showed an increase of the corrosion rate values, with decreasing pH and increasing concentration of H₂S generated by the thiosulphate. For the lowest H₂S concentrations and long test times, the corrosion process was inhibited, causing a significant decrease in the corrosion rate. This effect was associated with the formation of a partially protective film formed on the samples' surfaces in solutions with low H₂S concentration.

The solution 2, with the highest concentration of thiosulfate (10⁻² mol/L Na₂S₂O₃), showed the highest corrosion rate, and the welded joint showed higher corrosion rate in comparison with those presented by the base metal, for almost all conditions studied. In most cases, the heat affected zone (HAZ) showed a severe localised corrosion attack which was attributed to the microstructural characteristics of this region.

5. Acknowledgments

The authors wish to acknowledge the financial support of CAPES, FAPERJ and PUC-Rio.

6. References

- Ma H, Cheng X, Li G, Chen S, Quan Z, Zhao S, et al. The influence of hydrogen sulphide on corrosion of iron under different conditions. *Corros Sci.* 2000;42:1669-83.
- Tang J, Shao Y, Guo J, Zhang T, Meng G, Wang F. The effect of H₂S concentrations behavior of carbon steel at 90°C. *Corros Sci.* 2010;52:2050-8.
- Carneiro RA, Ratnapuli RC, Lins VFC. The influence of chemical composition and microstructure of API linepipe steels on hydrogen induced cracking and sulphide stress corrosion cracking. *Mater Sci Eng A.* 2003;357:104-10.
- Park GT, Koh SU, Jung HG, Kim KY. Effect of microstructure on the hydrogen trapping efficiency and hydrogen induced cracking of line pipe steel. *Corros Sci.* 2008;50:1865-71.
- Inohara Y, Ishikawa N, Endo S. Recent development in high strength linepipe for sour environment. In: *Proceedings of the 13th International Offshore and Polar Engineering Conference*; 2003 May 25-20; Honolulu, Hawaii. *Proceedings. Cupertino: International Society of Offshore and Polar Engineers (ISOPE)*; 2003, p. 60-66.
- Koh SU, Kim JS, Yang BY, Kim KY. Effect of line pipe steel microstructure on susceptibility to sulphide stress cracking. *Corrosion.* 2004;60:244.
- Ballesteros AF, Ponciano JAC, Bott IS. Susceptibility of pipeline girth welds to hydrogen embrittlement and sulphide stress cracking. *Materials and Corrosion.* 2012;63:9999. <http://dx.doi.org/10.1002/maco.201206574>.
- Bott IS, Souza LFG, Teixeira JCG, Rios PR. High strength HTP steel development for pipelines: a Brazilian perspective. *Metal Mat Trans A.* 2005;36A:443-54.
- Ren C, Liu D, Bai Z, Li T. Corrosion behavior of oil tube steel in stimulant solution with hydrogen sulphide and carbon dioxide. *Mater Chem Phys.* 2005;93:305-9.
- Lu BT, Luo JL. Relationship between yield strength and near neutral pH stress corrosion cracking resistance of pipeline steels - An effect of microstructure. *Corros Sci.* 2006;62(2):129-40.
- Albarran JL, Martinez L, Lopez HF. Effect of heat treatment on the stress corrosion resistance of the microalloyed pipelines steel. *Corros Sci.* 1999;41:1037-49.
- Bulger J, Lou J. Effect of microstructure on near-neutral pH SCC. In: *International Pipeline Conference*; 2000 Oct 1-5; Calgary. *Proceedings.* New York: ASME; 2000.
- Leyer J, Sutter P, Marchevis H, Bosch C, Kulgemeyer A, Orleans JBJ. SSC resistance of a 125 Ksi steel grade in slightly sour environments. *NACE - International Corrosion Conference Series.* 2005;2005:05088.
- Natividad C, Salazar M, Garcia R, Gonzalez-Rodriguez JG, Perez R. Sulphide stress cracking behavior of weldments produced by indirect electric arc welding. *Corros Eng Sci Technol.* 2006;41(1):91-5.
- Natividad C, Salazar M, Contreras A, Albita A, Pérez R, Gonzalez-Rodriguez JG. Sulphide stress cracking susceptibility of X-60 and X-65 steel weldments. *Corrosion.* 2006;62(5):375-82.
- Beavers JA, Jonson JT, Sutherby RL. Materials factors influencing the initiation of near-neutral pH SCC on underground pipelines. In: *International Pipeline Conference*; 2000 Oct 1-5; Calgary. *Proceedings.* New York: ASME; 2000. p. 979-988.
- Omweg GM, Frankel GS, Bruce WA, Ramirez JE, Koch G. Effect of welding parameters and H₂S partial pressure on the susceptibility of welded HSLA steel to sulphide stress cracking. *Welding Research.* 2003;82(6):136-143.
- Sardico JB, Pitts RE. Corrosion of iron in an H₂S-CO₂-H₂O system composition and protectiveness of the sulfide film as a function off pH. *Corrosion.* 1965;21(11):350-4.
- ASTM: American Society for Testing and Materials. ASTM G1 - 03 (Reapproved 2011): standard practice for preparing, cleaning, and evaluating corrosion test specimens. West Conshohocken: ASTM; 2012.
- ASTM: American Society for Testing and Materials. ASTM G59-97: Standard practice for conducting potentiodynamic polarization resistance measurements. West Conshohocken: ASTM; 2003.
- Kane RD. Roles of H₂S in behaviour of engineering alloys. *International Metals Reviews.* 1985;30(6):291-301.
- ASTM: American Society for Testing and Materials. ASTM D2688 - 11: standard test method for corrosivity of water in the absence of heat transfer (weight loss method). West Conshohocken: ASTM; 2011.
- Zhou C, Zheng S, Chen C, Lu G. The effect of the partial pressure of H₂S on the permeation of hydrogen in the low carbon pipelines steel. *Corros Sci.* 2013;67:184-92.
- Lucio-Garcia MA, Gonzalez-Rodriguez JG, Casales M, Martinez L, Chacon-Nava JG, Neri-Flores MA, et al. Effect of heat treatment on H₂S corrosion of micro-alloyed C-Mn Steel. *Corros Sci.* 2009;51:2380-6.
- Ballesteros AF, Ponciano JAC, Bott IS. Corrosion evaluation of SAW Welded API 5L X-80 joints in H₂S-containing solution. *Mater Res.* 2015;18:417-26.
- Choi YS, Nestic S, Ling S. Effect of H₂S on the CO₂ corrosion of carbon steel in acidic solutions. *Electrochim Acta.* 2011;56:1752-60.
- Fragiel B, Serna S, Perez R. Electrochemical study of two microalloyed pipeline steels in H₂S environments. *Int J Hydrogen Energy.* 2005;30:1303-9.
- Arzola S, Mendoza J, Duran R, Genesca J. Electrochemical behavior of API X70 steel in hydrogen sulfide-containing solutions. *Corrosion.* 2006;62:433-42.
- Maddala J, Sambath K, Kumar V, Ramanahan S. Identification of reaction mechanism for anodic dissolution of metals using Electrochemical Impedance Spectroscopy. *J Electroanal Chem.* 2010;638:183-8.